Supporting Information

for

Cation-Exchanged Zeolites for the Selective Oxidation of Methane to Methanol

Ambarish R. Kulkarni,[a,b,*] Zhi-Jian Zhao,[a,b,c] Samira Siahrostami,[a,b] Jens K. Nørskov,[a,b] Felix Studt [d,e*]

[a] SUNCAT Center for Interface Science and Catalysis, Department of Chemical Engineering, Stanford University, 450 Serra Mall Stanford, California 94305, USA

[b] SUNCAT Center for Interface Science and Catalysis, SLAC National Accelerator Laboratory, Menlo Park, California 94025, United States

[c] Key Laboratory for Green Chemical Technology of Ministry of Education, Collaborative Innovation Center of Chemical Science and Engineering, School of Chemical Engineering and Technology, Tianjin University, Tianjin 300072, People's Republic of China

[d] Institute of Catalysis Research and Technology, Karlsruhe Institute of Technology, Hermann-von-Helmholtz-Platz 1, 76344 Eggenstein-Leopoldshafen, Germany

[e] Institute for Chemical Technology and Polymer Chemistry, Karlsruhe Institute of Technology, Engesserstr. 18, 76131 Karlsruhe, Germany

E-mail: felix.studt@kit.edu, ambarish@stanford.edu.

KEYWORDS: Partial methane oxidation, Density Functional Theory, zeolites

Table S1. Table showing the improvements in productivity (in mol-methanol/mol-Cu) of Cu-exchanged zeolites from 2005 to 2017, used in Table 1.

Date	Zeolite	Oxidant	Productivity	Si/Al	Comments	Ref
15-Jan-05	MFI	O_2	0.020	12	First report claiming bis(μ-oxo)dicopper as the active site. UV-vis band at 22,700 cm-1	1
	MOR	O_2	0.020	8.8		
	FAU	O_2	0.005	2.7		
26-Oct-05	MOR	O_2	0.007	8.8	UV-vis band at 22,000 cm-1 for MOR. EMT, FAU, FER and BEA at inactive at lower reaction temperatures.	2
	EMT	O_2	0.001	4		
	FAU	O_2	0.007	2.7 – 37		
	FER	O_2	0.001	6.2		
	BEA	O_2	0.002	9.8		
	MFI	O_2	0.012	12	Higher reaction temperature gives better productivity	
	MOR	O_2	0.020	8.8		
	FER	O_2	0.013	6.2		
	BEA	O_2	0.006	9.8		
10-Nov-09	MFI	N_2O	0.021	12	Active site identified as mono(μ-oxo)dicopper	3
4-Jun-10	MFI	O_2	0.006	17.5	Polar and protic solvents for methanol extraction	4
11-Nov-11	MOR	O_2	0.020	11	Steam/ water saturated He for methanol extraction	5
7-Aug-14	MFI	NO	0.002	1.88	NO as an oxidant	6
4-Feb-15	CHA	O_2	0.060	6, 12	Small 8MR zeolites shown to be active.	7
	SAPO-34	O_2	0.010	6		
	AFX	O_2	0.050	6.5		
	AEI	O_2	0.090	10		
	MOR	O_2	0.040	5		
	MFI	O_2	0.030	11.5		
25-Jun-15	MOR	O_2	0.300	5.5 - 21	Tri-copper active site	8
8-Mar-16	MOR	O_2	0.031	4.1	Different synthesis techniques	9
	MOR	O_2	0.047	3.1		
24-Mar-16	MOR	O_2	0.139	4.7	Low temperature, isothermal process. Dehydrated copper oxide clusters as the active site	10
	MOR	O_2	0.076	4.7		
	MFI	O_2	0.040	2.8		
	FAU	O_2	0.009	7.6		
13-Jun-16	MFI	O_2	0.090	13.2	First report of a continuous process for methane activation	11
	MFI	O_2	0.200	13.6		
1-Aug-16	MFI	O_2	0.180	0 – 0.67	Paired and isolated Al sites in MFI for tri-copper active sites	12
	MFI	O_2	0.200	0 – 0.54		
21-Oct-16	CHA	N_2O	0.026	12	Continuous process for methane activation in SSZ-13	13
	CHA	N_2O	0.060	12		
	CHA	N_2O	0.071	12		
	CHA	O_2	0.018	12		
	CHA	O_2	0.038	12		
	CHA	O_2	0.091	12		
25-Dec-16	MOR	O_2	0.230	11	Effect of pH, co-cations	14
3-Jan-17	MOR	O_2	0.146	10	Solid state ion-exchange vs. aqueous phase ion-exchange	15
	MOR	O_2	0.063	10		
	MOR	O_2	0.224	10		
22-Mar-17	MOR	O_2	0.220	20	O_2 activation at very high temperatures	16
	MOR	N_2O	0.310	20		
4-May-17	MOR	H_2O	0.250	13	Methane activation using H_2O as an oxidant	17
25-Sep-17	CHA	O_2	0.202	12	Systematic exploration of process parameters, $[Cu\text{-}OH]^+$ is the precursor to the active site in CHA	18

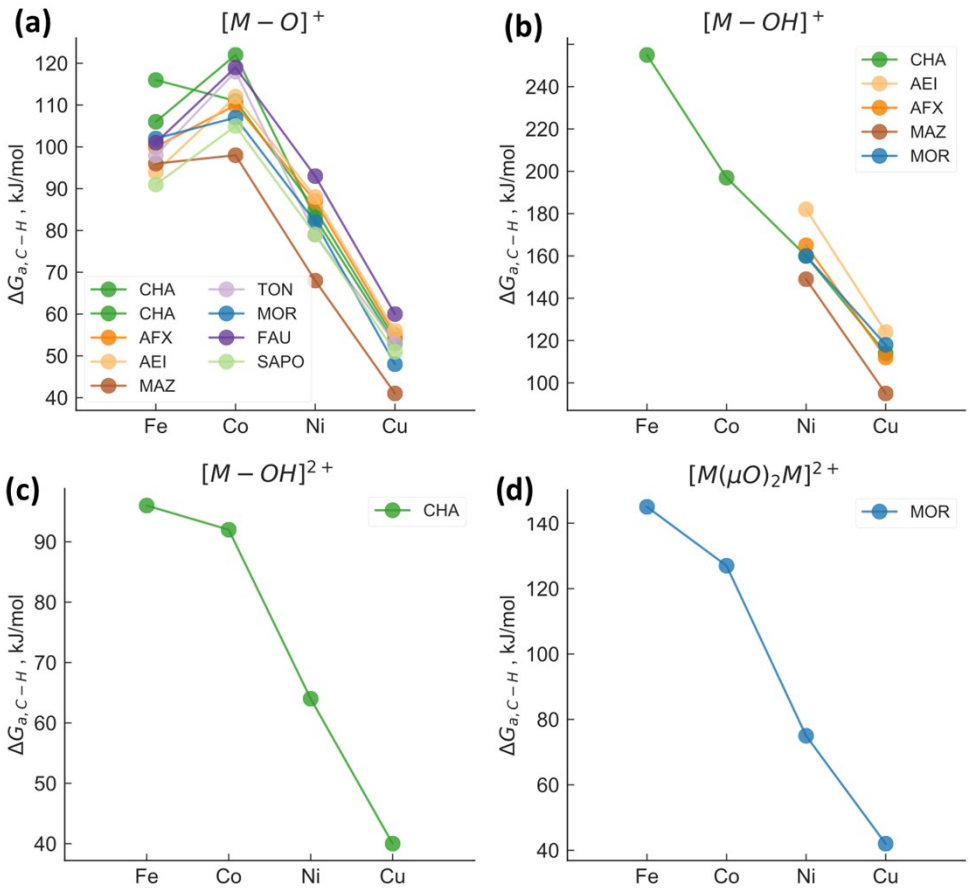

Figure S1. Effect of changing transition metal cation on the calculated methane activation barriers for (a) $[M\text{-}O]^+$, (b) $[M\text{-}OH]^+$, (c) $[M\text{-}OH]^{2+}$ and (d) $[M(\mu O)_2M]^{2+}$ motifs in different zeolites.

Table S2. Formation energy ($\Delta E_{f,DFT}$) and transition state energy ($\Delta E_{a,DFT}$) of $[M\text{-}O]^+$ motif in CHA. In contrast to other cations, DFT predicts a low spin state configuration of $[Fe\text{-}O]^+$ the TS. This results in $[Fe\text{-}O]^+$ having a lower C-H activation barrier than $[Co\text{-}O]^+$ as shown in Fig 3b.

Cation	$\Delta E_{f,DFT}$ (eV)	# unpaired electrons	$\Delta E_{a,DFT}$ (eV)
Fe_high	-2.29	3	0.84
Fe_low	-2.09	5	1.02
Co	-1.74	4	0.79
Ni	-0.95	3	0.52
Cu	0.09	2	0.20

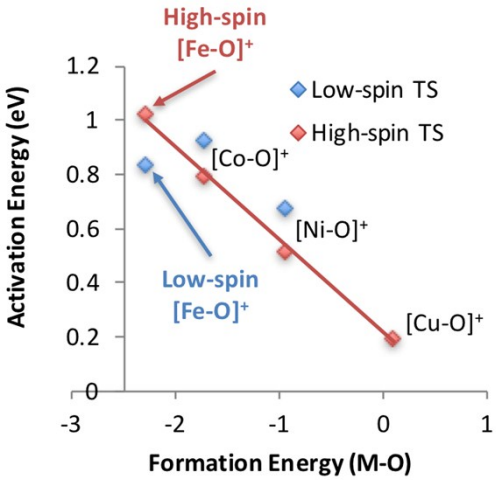

Figure S2. Scaling lines for the high-spin (red) and low-spin (blue) transition states for various $[M\text{-}O]^+$ motifs in CHA. Activation energies are calculated relative to the most stable high (Co, Ni and Cu) or low (Fe) states for $[M\text{-}O]^+$.

Table S3. Transition state free energies and ∠Cu-O-Cu for $[Cu\text{-}O\text{-}Cu]^{2+}$ motifs in CHA, MOR, FAU and MFI topologies.

Framework Topology	Cu-O-Cu angle	$\Delta G_{a,C\text{-}H}$ (kJ/mol)
CHA	115°	94
MOR	135°	104
FAU	126°	105
MFI	135.8°	98

Table S4. Bader charges of the active oxygen atoms for various Cu-motifs in MOR.

Motif/MOR	q_{bader}
$[Cu\text{-}O]^+$	-0.4
$[bis(\mu\text{-}oxo)Cu]^{2+}$	-0.55 [a]
$[Cu_3(\mu O_3)]^{2+}$	-0.7 [a]
$[Cu\text{-}OH]^+$	-1.4
$[Cu\text{-}O\text{-}Cu]^{2+}$	-0.8
$[Cu_6O_7]^{2+}$	-0.8 [a]

[a] averaged over all oxygen atoms of the motif

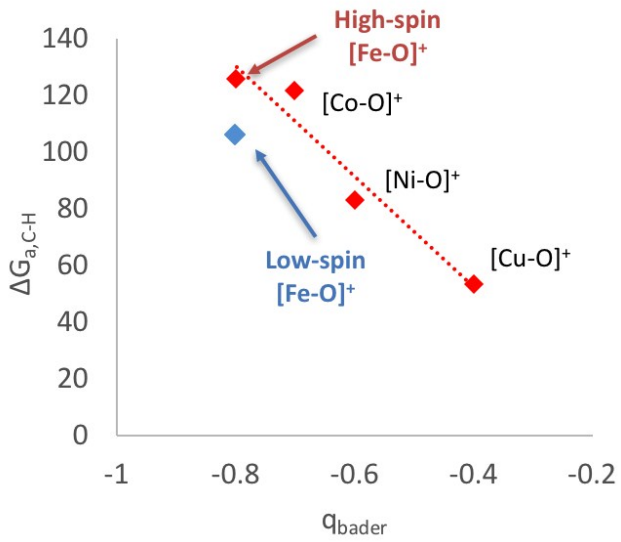

Figure S3. Correlation between the Bader charge on the active oxygen and the activation free energy ($\Delta G_{a,C\text{-}H}$) for $[M\text{-}O]^+$ motifs in CHA. As discussed above, the low-spin configuration of $[Fe\text{-}O]^+$ is more favorable than the high-spin configuration.

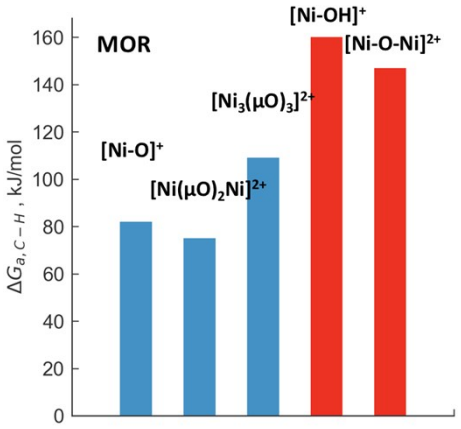

Figure S4. Activation free energy ($\Delta G_{a,C\text{-}H}$) for various Ni motifs in MOR. The motifs with high (low) reactivity are shown in blue (red).

Table S5 Free energy corrections (in kJ/mol) of transition states of different motifs at 423 K. Details for individual motifs are shown in Table S9. The equation $\Delta G = \Delta E_{DFT} + ZPE + \Delta(C_p dT - TdS)$ is used calculating the free energies.

	Total Contributions $\Delta G - \Delta E_{DFT}$
$[M\text{-}O]^{1+,\,2+}$	34.8
$[M\text{-}OH]^{1+,\,2+}$	37.3
$[M\text{-}O\text{-}M]^{2+}$	35.5
$[M(\mu O)_2M]^{2+}$	25.4
$[M_3(\mu O)_3]^{2+}$	27.1
$[Cu_6O_7]^{2+}$	36.6

Table S6. Free energy corrections (in kJ/mol) for calculating the formation energies of various motifs at 723 K. Details for individual motifs are shown in Table S9. The equation $\Delta G = \Delta E_{DFT} + ZPE + \Delta(C_p dT - TdS)$ is used calculating the free energies.

	Total Contributions $\Delta G - \Delta E_{DFT}$
$[M\text{-}O]^{1+,\,2+}$	61.3
$[M\text{-}OH]^{1+,\,2+}$	86.0
$[M\text{-}O\text{-}M]^{2+}$	68.1
$[M(\mu O)_2M]^{2+}$	58.5
$[M_3(\mu O)_3]^{2+}$	63.2
$[Cu_6O_7]^{2+}$	60.9

Table S7. Free energy corrections (in kJ/mol) for methanol and water adsorption at 523 K. Details of different motifs and cations are shown in Table S9. The equation $\Delta G = \Delta E_{DFT} + ZPE + \Delta(C_p dT - TdS)$ is used calculating the free energies.

	Total Contributions $\Delta G - \Delta E_{DFT}$
Methanol	106.1
Water	81.1

CALCULATION OF METHANE ACTIVATION RATES

Using T = 423 K, partial pressure of methane ($P_{methane}$)= 1 bar and activation free energy of 115 kJ/mol, we use,

$$k_{C-H} = \frac{k_B T}{h} e^{\frac{\Delta G_{a,C-H}}{k_B T}}$$

to get k_{C-H} = 0.055 s^{-1}. Assuming first order kinetics in methane, the rate of methane consumption ($r_{methane}$) is given as:

$r_{methane} = -k_{C-H} * P_{methane} * \theta$, where θ is the coverage of active site motifs (say $[M\text{-}O]^+$ species). Using standard first-order rate law analysis ($t = -\frac{ln[\theta_{final}]}{k}$) and assuming that the partial pressure of methane doesn't change, we predict ~ 1 min for 99% of the motifs to be reacted (forming $[M\text{-}OH]^+$ in the above example). Note that the chosen threshold $\Delta G_{a,C\text{-}H}$ (115 kJ/mol) is close to the upper bound of experimentally measured activation energies (100 kJ/mol[11] and 142 kJ/mol[13]).

CHOICE OF REFERENCE STATES

Cation-exchanged zeolites are typically synthesized by aqueous phase cation exchange with a Na- or a H- form of the parent material.[7] In this situation, the transition metal salt (say acetate, nitrate etc.) is used as the TM source, and metal oxide phases are not typically formed. Thus, we use the 'bare' cation exchanged form of the zeolite as a reference, rather than the TM oxide.[8, 19] This allows us to compare the 'stability' of a given motif for different cations, which is not possible if oxides were used as a reference (i.e. no way to compare CuO with Fe_3O_4, Co_3O_4, NiO etc.).

However, this also implies that the relative stability of different motifs can only be compared if the number of Al remains the same in the reference. Specifically, we used the following equations to calculate the formation energies of various motifs, where Z_1 and Z_2 represent the zeolite with one or two Al atoms, respectively.

(1) $Z_1\text{-}M + 0\ H_2O + 0.5\ O_2 \rightarrow Z\text{-}[M\text{-}O]^+$

(2) $Z_2\text{-}M + 0\ H_2O + 0.5\ O_2 \rightarrow Z\text{-}[M\text{-}O]^{2+}$

(3) Z_1-M + 0.5 H_2O + 0.25 O_2 → Z-$[M\text{-}OH]^+$

(4) Z_2-M + 0.5 H_2O + 0.25 O_2 → Z_2-$[M\text{-}OH]^{2+}$

(5) Z_2-2M + 0 H_2O + 0.5 O_2 → Z_2-$[M\text{-}O\text{-}M]^{2+}$

(6) Z_2-2M + 0 H_2O + 1 O_2 → Z_2-$[M\text{-}(\mu O)_2\text{-}M]^{2+}$

(7) Z_2-(M_3O_2) + 0 H_2O + 0.5 O_2 → Z_2-$[M_3(\mu O)_3]^{2+}$

(8) Z_2-(M_6O_6) + 0 H_2O + 0.5 O_2 → Z_2-$[M_6O_7]^{2+}$

Based on the above equations, the following sets of motifs can be compared directly (if the Al positions are also the same).

Set 1: $[M\text{-}O]^+$, $[M\text{-}OH]^+$

Set 2: $[M\text{-}O]^{2+}$, $[M\text{-}OH]^{2+}$, $[M\text{-}O\text{-}M]^{2+}$, $[M\text{-}(\mu O)_2\text{-}M]^{2+}$

Set3: $[M_3(\mu O)_2]^{2+}$

Set4: $[M_6O_7]^{2+}$

Since the $[M_3O_3]^{2+}$ and $[M_6O_7]^{2+}$ motifs contain more cations than the number of Al atoms in the zeolite, additional BrønstedH form of the zeolites (Z_2-2H) need to be included[20] to compare them with other Z_2/2Al systems as shown below.

(9) 1.5 Z_2-2M -0.5 $\underline{Z_2\text{-}2H}$ + 0.5 H_2O + 1.25 O_2 → Z_2-$[M_3(\mu O)_3]^{2+}$

(10) 3 Z_2-2M - 2 $\underline{Z_2\text{-}2H}$ + 2 H_2O + 2.5 O_2 → Z_2-$[M_6O_7]^{2+}$

However, these equations now require different number of BronstedH for different cations and their most stable oxidation states (3 for Fe^{+3}, 2 for Co^{+2}, 1 for Cu^+ etc), which prevents the comparison among different metals. Moreover, the results get skewed by the high formation energies of BronstedH and depend on 'favorable' Al positions for different cations (not shown). This complex, system-specific analysis is better suited for detailed studies focusing on a single TM cations. As the focus of this work is to rationalize overall trends, we chose to not include the 'bare' cation reference for the more complex motifs.

The equations #7 and #8 calculate the 'binding energy' of the active oxygen, which can be compared across different cations. This, in essence, is similar to the motivation of equations #1 - #6, which are just the 'binding energies' of various active oxygen species.

We highlight that while the choice of the reference state for different motifs is somewhat arbitrary, the general conclusion that stability and activity are inversely correlated seems to hold over all the motifs and materials considered here.

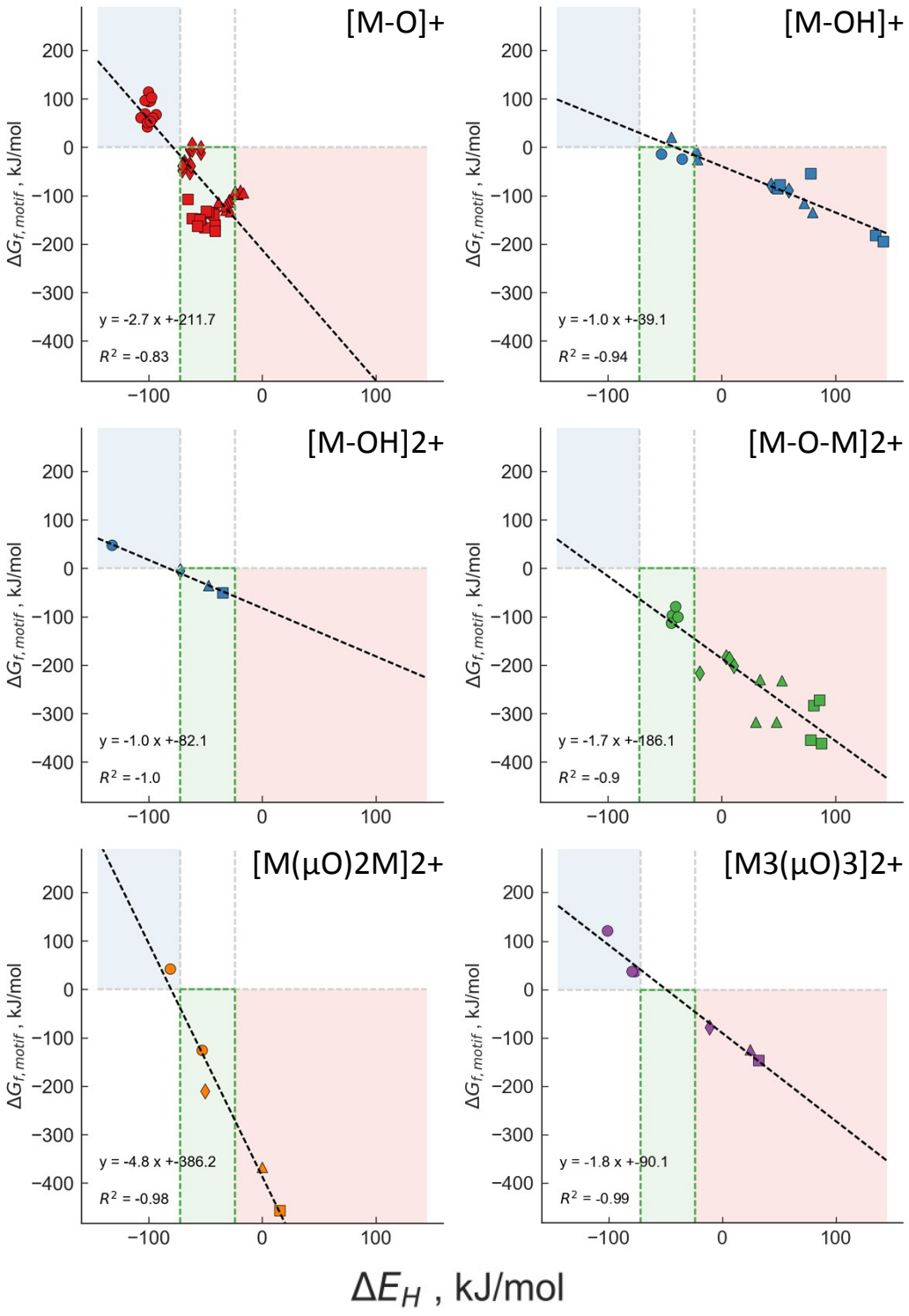

Figure S5. Relationship between formation free energies (ΔG_f) and hydrogen affinity (ΔE_H) for various motifs plotted separately. Although a clear correlation is seen for a given motif, the equations for different motifs are different because of definitions of the reference states.

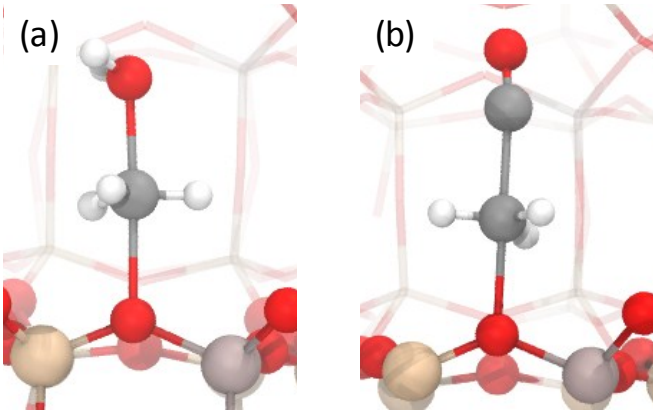

Figure S6. Transition states and free energy barriers for reaction of framework-bound methoxy group with (a) water and (b) CO. The reaction with water forms a protonated methanol that deprotonates to from a Brønsted H and the methanol product. When CO is included the extraction process, the acetyl intermediate is initially formed. This is further hydrolyzed with water to form acetic acid, as reported by Narsimhan et al.[21]

Table S8. Binding energies of methanol for $[M\text{-}O\text{-}M]^{2+}$ and $[M_3(\mu O)_3]^{2+}$ motifs in MOR.

Motif	**Methanol binding Energy** [a]
$[Co\text{-}O\text{-}Co]^{2+}$	-129
$[Ni\text{-}O\text{-}Ni]^{2+}$	-94
$[Cu\text{-}O\text{-}Cu]^{2+}$	-100
$[Cu_3(\mu O)_3]^{2+}$	-74, -100, -132 [b]

[a] desorption involves removal of the active oxygen as methanol based on the reaction: [M-CH3OH-M] → [M-*-M] + CH3OH, where * represents the empty oxygen site.

[b] different binding sites

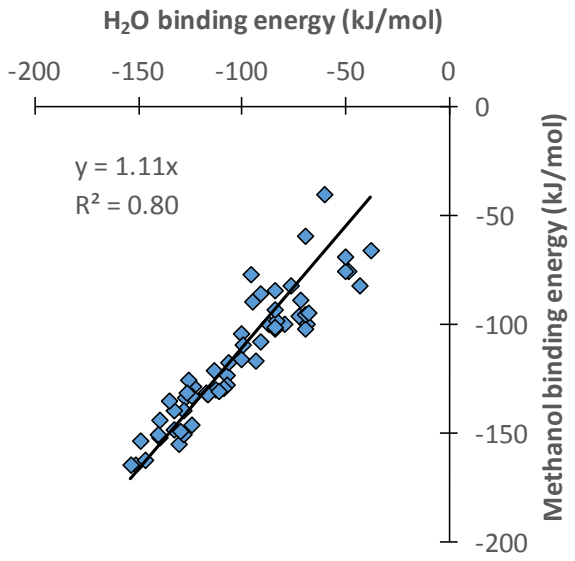

Figure S7. Linear relationship between the binding energy of water and methanol for different cations, topologies and binding sites. The intercept has been fixed at (0,0) during the linear regression. The figure shows the calculated DFT energies, without including entropic and finite temperature contributions.

CALCULATION OF THEORETICAL CAPACITY

Consider a CHA zeolite with Si/Al = 11 and Cu/Al = 1, with the $[Cu\text{-}OH]^+$ as the active species. In this hypothetical example 100% of the Cu atoms exist at the active site. However, we have previously shown that this number is ~ 5 – 12% in a real CHA.[22] However, for the purposes of calculating the theoretical capacity, let us consider that only $[Cu\text{-}OH]^+$ species are allowed to be formed. For a 36-atom unit cell, the individual atoms we get the density as 799.5 g/uc, and for each $[Cu\text{-}OH]^+$ we get one methanol being formed. As shown below, this corresponds to 1,250 μmol/g-catalyst (or, equivalently 0.04 g-methanol/g-catalyst).

Element	# of atoms	atomic mass	total mass
Si	11	28	308
Al	1	27	27
O	24	16	384
Cu	1	63.5	63.5
(OH)	1	17	17
		Total (g/mol-uc)	**799.5**

1 mol of methanol / uc of CHA	
1	mol ch3oh per 799.5 g catalyst
0.001250782	mol ch3oh per g cat
1250.781739	micro-mol-ch3oh/g cat
1.250781739	mmol/g cat
0.001250782	mol/g cat
0.040025016	g/ g cat
0.040025016	**kg ch3oh/ kg cat**

Table S9. Total entropy contributions for individual motifs and cations for transition states (at 423 K), motif formation (At 723 K), methanol and water adsorption (at 523 K). The equation $\Delta G = \Delta E_{DFT} + ZPE + \Delta(C_p dT - TdS)$ is used calculating the free energies. The systems for which the corrections were not evaluated are denoted by n/a, and significant differences are not expected.

CHA [M-O]$^+$/6MR	Total Contributions, $\Delta G - \Delta E_{DFT}$ (in eV)			
	Transition state (423 K)	Motif formation (723 K)	CH_3OH adsorption (523 K)	H_2O adsorption (523 K)
Fe	0.38	0.62	1.07	0.76
Co	0.33	0.65	1.03	0.88
Ni	0.38	0.59	1.06	0.90
Cu	0.38	0.61	1.04	0.90

CHA [M-O]$^+$/8MR	Total Contributions, $\Delta G - \Delta E_{DFT}$ (in eV)			
	Transition state (423 K)	Motif formation (723 K)	CH_3OH adsorption (523 K)	H_2O adsorption (523 K)
Fe	0.37	n/a	n/a	n/a
Co	0.29	0.64	1.03	0.87
Ni	0.33	n/a	n/a	n/a
Cu	0.34	0.70	1.10	1.01

TON [M-O]$^+$/10MR	Total Contributions, $\Delta G - \Delta E_{DFT}$ (in eV)			
	Transition state (423 K)	Motif formation (723 K)	CH_3OH adsorption (523 K)	H_2O adsorption (523 K)
Fe	n/a	0.67	n/a	0.67
Co	n/a	n/a	0.98	0.77
Ni	0.45	n/a	1.09	0.76
Cu	0.35	n/a	1.07	0.87

FAU [M-O]$^+$/12MR	Total Contributions, $\Delta G - \Delta E_{DFT}$ (in eV)			
	Transition state (423 K)	Motif formation (723 K)	CH_3OH adsorption (523 K)	H_2O adsorption (523 K)
Fe	n/a	0.60	1.07	n/a
Co	n/a	n/a	n/a	n/a
Ni	n/a	n/a	0.92	n/a
Cu	n/a	n/a	n/a	n/a
MOR [M-O]$^+$/12MR	Total Contributions, $\Delta G - \Delta E_{DFT}$ (in eV)			

	Transition state (423 K)	Motif formation (723 K)	CH_3OH adsorption (523 K)	H_2O adsorption (523 K)
Fe	0.36	0.62	0.99	n/a
Co	0.35	0.58	1.06	n/a
Ni	0.37	0.63	1.01	n/a
Cu	0.37	0.65	1.01	n/a

CHA **$[M\text{-}OH]^+$/8MR**	Total Contributions, $\Delta G - \Delta E_{DFT}$ (in eV)			
	Transition state (423 K)	Motif formation (723 K)	CH_3OH adsorption (523 K)	H_2O adsorption (523 K)
Fe	n/a	n/a	n/a	n/a
Co	n/a	0.85	n/a	n/a
Ni	0.40	n/a	n/a	n/a
Cu	0.37	0.99	n/a	n/a

MOR **$[M\text{-}O\text{-}M]^{2+}$/8MR**	Total Contributions, $\Delta G - \Delta E_{DFT}$ (in eV)			
	Transition state (423 K)	Motif formation (723 K)	CH_3OH adsorption (523 K)	H_2O adsorption (523 K)
Fe	0.45	0.68	n/a	n/a
Co	0.37	0.72	n/a	n/a
Ni	0.36	0.71	n/a	n/a
Cu	0.30	0.71	n/a	n/a

MOR **$[M(\mu O)_2M]^{2+}$/8MR**	Total Contributions, $\Delta G - \Delta E_{DFT}$ (in eV)			
	Transition state (423 K)	Motif formation (723 K)	CH_3OH adsorption (523 K)	H_2O adsorption (523 K)
Fe	n/a	n/a	n/a	n/a
Co	0.22	n/a	n/a	n/a
Ni	0.30	0.61	n/a	n/a
Cu	0.26	0.61	n/a	n/a

MOR **$[M_3O_3]^{2+}$/8MR**	Total Contributions, $\Delta G - \Delta E_{DFT}$ (in eV)			
	Transition state (423 K)	Motif formation (723 K)	CH_3OH adsorption (523 K)	H_2O adsorption (523 K)
Fe	n/a	n/a	n/a	n/a
Co	n/a	n/a	n/a	n/a
Ni	0.26	0.67	n/a	n/a
Cu	0.30	0.63	n/a	n/a

MOR $[Cu_3O_7]^{2+}$/8MR	Total Contributions, $\Delta G - \Delta E_{DFT}$ (in eV)			
	Transition state (423 K)	Motif formation (723 K)	CH_3OH adsorption (523 K)	H_2O adsorption (523 K)
Cu	0.38	0.63	1.04	n/a

References

1. M. H. Groothaert, P. J. Smeets, B. F. Sels, P. A. Jacobs and R. A. Schoonheydt, *Journal of the American Chemical Society*, 2005, **127**, 1394-1395.
2. P. J. Smeets, M. H. Groothaert and R. A. Schoonheydt, *Catalysis Today*, 2005, **110**, 303-309.
3. J. S. Woertink, P. J. Smeets, M. H. Groothaert, M. A. Vance, B. F. Sels, R. A. Schoonheydt and E. I. Solomon, *Proc. Natl. Acad. Sci.*, 2009, **106**, 18908-18913.
4. N. V. Beznis, B. M. Weckhuysen and J. H. Bitter, *Catalysis Letters*, 2010, **138**, 14-22.
5. E. M. Alayon, M. Nachtegaal, M. Ranocchiari and J. A. van Bokhoven, *Chemical Communications*, 2012, **48**, 404-406.
6. T. Sheppard, C. D. Hamill, A. Goguet, D. W. Rooney and J. M. Thompson, *Chemical Communications*, 2014, **50**, 11053-11055.
7. M. J. Wulfers, S. Teketel, B. Ipek and R. F. Lobo, *Chemical Communications*, 2015, **51**, 4447-4450.
8. S. Grundner, M. A. C. Markovits, G. Li, M. Tromp, E. A. Pidko, E. J. M. Hensen, A. Jentys, M. Sanchez-Sanchez and J. A. Lercher, *Nat. Commun.*, 2015, **6**.
9. S. E. Bozbag, E. M. C. Alayon, J. Pechacek, M. Nachtegaal, M. Ranocchiari and J. A. van Bokhoven, *Catalysis Science & Technology*, 2016, **6**, 5011-5022.
10. P. Tomkins, A. Mansouri, S. E. Bozbag, F. Krumeich, M. B. Park, E. M. C. Alayon, M. Ranocchiari and J. A. van Bokhoven, *Angewandte Chemie*, 2016, **128**, 5557-5561.
11. K. Narsimhan, K. Iyoki, K. Dinh and Y. Román-Leshkov, *ACS Central Science*, 2016, **2**, 424-429.
12. M. A. C. Markovits, A. Jentys, M. Tromp, M. Sanchez-Sanchez and J. A. Lercher, *Top Catal*, 2016, **59**, 1554–1563.
13. B. Ipek and R. F. Lobo, *Chemical Communications*, 2016, **52**, 13401-13404.
14. S. Grundner, W. Luo, M. Sanchez-Sanchez and J. A. Lercher, *Chemical Communications*, 2016, **52**, 2553-2556.
15. H. V. Le, S. Parishan, A. Sagaltchik, C. Göbel, C. Schlesiger, W. Malzer, A. Trunschke, R. Schomäcker and A. Thomas, *ACS Catal.*, 2017, **7**, 1403-1412.
16. Y. Kim, T. Y. Kim, H. Lee and J. Yi, *Chemical Communications*, 2017, DOI: 10.1039/C7CC00467B.
17. V. L. Sushkevich, D. Palagin, M. Ranocchiari and J. A. van Bokhoven, *Science*, 2017, **356**, 523.

18. D. K. Pappas, E. Borfecchia, M. Dyballa, I. Pankin, K. A. Lomachenko, A. Martini, M. Signorile, S. Teketel, B. Arstad and G. Berlier, *Journal of the American Chemical Society*, 2017.
19. G. Li, P. Vassilev, M. Sanchez-Sanchez, J. A. Lercher, E. J. Hensen and E. A. Pidko, *Journal of Catalysis*, 2016, **338**, 305-312.
20. B. Ipek, M. J. Wulfers, H. Kim, F. Göltl, I. Hermans, J. P. Smith, K. S. Booksh, C. M. Brown and R. F. Lobo, *ACS Catal.*, 2017, **7**, 4291–4303.
21. K. Narsimhan, V. K. Michaelis, G. Mathies, W. R. Gunther, R. G. Griffin and Y. Román-Leshkov, *Journal of the American Chemical Society*, 2015, **137**, 1825-1832.
22. A. R. Kulkarni, Z.-J. Zhao, S. Siahrostami, J. K. Nørskov and F. Studt, *ACS Catal.*, 2016, **6**, 6531-6536.